NÖHÜ Müh. Bilim. Derg. / NOHU J. Eng. Sci., Erken Görünüm / InPress
Niğde Ömer Halisdemir Üniversitesi Mühendislik Bilimleri Dergisi
Niğde Ömer Halisdemir University Journal of Engineering Sciences
Araştırma makalesi / Research article
www.dergipark.org.tr/tr/pub/ngumuh / www.dergipark.org.tr/en/pub/ngumuh

Superior adsorption performance of high temperature solvothermal synthesized zirconium metal-organic framework nanoparticles in dye removal

Yüksek sıcaklıkta solvotermal sentezlenen zirkonyum metal-organik kafes nanopartiküllerinin boya giderimindeki üstün adsorpsiyon performansı

Nergiz Kanmaz [1,*]

[1] *Chemical Engineering Department, Engineering Faculty, Yalova University, Yalova, Türkiye.*

Abstract

In the present study, a zirconium-based metal-organic framework (UiO-66) nanoparticle was synthesized by solvothermal technique and characterized by FT-IR, XRD, SEM, BET analyses and zeta potential measurements. The effectiveness of UiO-66 nanoparticles for crystal violet (CV) adsorption was examined. CV removal process reached equilibrium in 30 min and the system was consistent with the pseudo-second-order model, which involves chemical reactions. The equilibrium results were compatible with the Dubinin-Raduskevich isotherm model. The maximum monolayer adsorption capacity was calculated as 998.18 mg g−1. It was deduced that CV removal rate was low when the solution pH was acidic, and surface charge was dominant in adsorption. In thermodynamic analysis, CV adsorption process is exothermic and spontaneous. The reusability of UiO-66 was investigated and 80.04% CV removal was obtained even after 5 successful cycles. According to the results, UiO-66 nanoparticles have a promising potential for rapid and efficient removal of CV dye.

Keywords: UiO-66, Adsorption, Desorption, Crystal violet.

Öz

Bu çalışmada, zirkonyum esaslı metal-organik kafes (UiO-66) nanopartikülü solvotermal teknikle sentezlenmiş ve FT-IR, XRD, SEM, BET analizleri ve zeta potansiyeli ölçümleri ile karakterize edilmiştir. UiO-66 nanopartiküllerinin kristal viyole (CV) adsorpsiyonu için etkinliği incelenmiştir. CV giderme işlemi 30 dakikada dengeye ulaşmıştır ve sistem kimyasal reaksiyonları içeren yalancı-ikinci dereceden modelle tutarlıdır. Denge sonuçları Dubinin-Raduskevich izoterm modeliyle uyumludur. Maksimum tek katmanlı adsorpsiyon kapasitesi 998.18 mg g^{-1} olarak hesaplanmıştır. Çözelti pH'ı asidik olduğunda CV giderme oranının düşük olduğu ve adsorpsiyonda yüzey yükünün baskın olduğu sonucuna varılmıştır. Termodinamik analizde CV adsorpsiyon işlemi ekzotermik ve kendiliğinden gerçekleşmektedir. UiO-66'nın tekrar kullanılabilirliği araştırılmış ve 5 başarılı çevrimden sonra bile %80.04 CV giderimi elde edilmiştir. Elde edilen sonuçlara göre, UiO-66 nanopartikülleri CV boyasının hızlı ve etkili bir şekilde giderilmesi için ümit verici bir potansiyele sahiptir.

Anahtar kelimeler: UiO-66, Adsorpsiyon, Desorpsiyon, Krsital viyole.

1 Introduction

Human activities increased with the progress of industrialization, and organic pollutants from manufacturing processes have resulted in serious water pollution issues [1]. Every year, more than 10000 tons of dyes are released into marine environments worldwide, particularly in developing nations with essentially non-existent environmental protection standards [2]. In addition, dyes are not biodegradable when released into the environment; they affect the appearance of water, reduce oxygen solubility and prevent light from penetrating water [3]. Crystal violet (CV) is used for various purposes in areas such as textile, paper, indicator, fertilizer and detergent [4]. It is a frequently employed triphenylmethane organic dye that is hazardous to water life and human health due to its high toxicity and persistence in the environment. About 10% of CV production volume is discharged into ecosystems, which has a significant negative impact on environment. Concerns about the long-term negative effects of CV are raised by its capacity for bioaccumulation within ecosystems [5]. Obviously, it is crucial to eliminate CV from water mediums to protect the health of living organisms.

Numerous techniques are chosen to remove toxic organic dyes from wastewater. These techniques have been studied as photo-Fenton process [6], membrane separation [7], photocatalysis [8,9] and biodegradation [10]. Adsorption is a popular technique that is thought to be among the most competitive, easy to use, and produces no hazardous byproducts. It also accounts for its low cost and broad variety of applications [11]. A wide variety of materials are used as adsorbents in wastewater treatment. Commonly favored adsorbent materials in industrial water remediation are reported as clays [12], activated carbons [13], zeolites [14] and hydrogels [15]. Besides these, researchers are exploring and proposing novel and high performance advanced materials to be considered as adsorbents [16].

* Sorumlu yazar / Corresponding author, e-posta / e-mail:nergizkanmaz@gmail.com (N. Kanmaz)
Geliş / Recieved: 06.12.2024 Kabul / Accepted: 20.01.2025 Yayımlanma / Published: xx.xx.20xx
doi: 10.28948/ngumuh.1597274

Novel crystalline organic-inorganic porous hybrid materials designated metal-organic frameworks (MOFs) have garnered a lot of interest because of their high surface area, impressive tunability, and noteworthy adsorption properties [17] for the adsorption of various hazardous chemicals MOFs are involved in the removal of organic pollutants through various adsorption mechanisms such as hydrophobic interactions, π-π bonding, hydrogen bonding, and electrostatic forces [18,19]. Zirconium-based MOFs are characterized by their large surface areas and remarkable chemical stability in both acidic and alkaline environments [20]. The strong interactions between Zr-O clusters and ligands also impart notable robustness to this class of MOFs [20]. Moreover, UiO-66 (Universitetet i Oslo) has effective adsorption ability for various metals [21], antibiotics [1,19] and dye pollutants [22]. Zhao et al. used UiO-66-NH2 modified with guanidino chelating agent as an adsorbent for the removal of methylene blue, copper and lead from the aquatic environment. The surface area of UiO-66-Gd was determined as 574.94 m2 g-1 and it was reported that it removed the studied pollutants by reaching high adsorption capacities [23]. Lan et al. reported that Co-doped UiO-66 synthesized by them reached adsorption capacities of 628.93 mg g-1 and 1106.22 mg g-1 for malachite green and rhodamine B removal, respectively [24].

Inspired by previous research, the adsorption performance of UiO-66 on crystal violet, a cationic and toxic textile dye, should be investigated. In this study, CV was used as a target pollutant to measure the performance of UiO-66 prepared by solvothermal technique in wastewater treatment. The prepared UiO-66 was characterized by FT-IR, XRD, SEM, BET and zeta potential measurement analyses. In physicochemical investigations, CV concentration effect, isotherm model analysis, time effect, kinetic model analysis, pH effect and temperature effect were examined. This paper contributed a beneficial insight of the application of zirconium-based MOF nanoparticles with superior adsorption properties in water treatment.

2 Materials and method

2.1 Materials

Zirconium tetrachloride ($ZrCl_4$), terephthalic acid (H_2BDC), crystal violet (hexamethylpararosaniline chloride, $C_{25}H_{30}N_3Cl$) were purchased from Sigma Aldrich, HCl (37%), sodium hydroxide (NaOH), N,N-dimethyl formamide (DMF) and ethanol (100%) were obtained from Merck Chemicals.

2.2 UiO-66 synthesis

0.77 g $ZrCl_4$ and 0.5 g terephthalic acid were weighed into a beaker, 50 mL dimethylformamide (DMF) was added and stirred vigorously with a magnetic stirrer until completely dissolved. After complete dissolution, it is transferred to a Teflon container, placed in a hydrothermal reactor and kept at 220 °C for 24 hours (Figure1). The solvothermal synthesized UiO-66 was washed with DMF 3 times to remove the unreacted materials and dried in a vacuum oven at 100 °C for 24 hours.

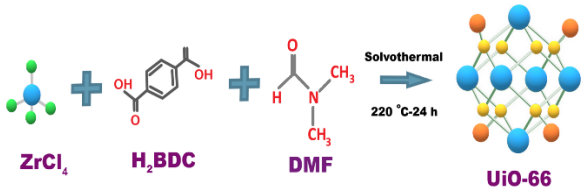

Figure 1. Solvothermal procedure of UiO-66 synthesis.

2.3 Characterization techniques

The surface morphology of zirconium-based MOF was obtained from scanning electron microscopy (SEM, Carl Zeiss 300VP). The functional groups of the sample were carried out by Fourier Transform-Infrared Spectroscopy (FT-IR, Perkin Elmer Spectrum 100) in the range of 4000-500 cm-1 wavenumber. X-Ray diffractometer (PANalytical X-Pert3 Powder) was utilized to determine crystalline structures. Micromeritics Gemini VII analyzer was utilized to determine the BET specific surface area of sample. Zeta potential measurements (Malvern Nano ZS) were obtained from different pH-adjusted suspensions.

2.4 Batch studies

The effect of solution pH was evaluated by adjusting of 10 mL 15 mg L^{-1} CV solutions between pH 2-10. Kinetic studies were performed for 5-90 min with 5 mg UiO-66 and 10 mL 15 mg L^{-1}. In the adsorption isotherm studies, 10 mL of CV solutions at concentrations of 15-300 mg L^{-1} (pH is around 5.2-5.7) were added onto the adsorbents, and the suspensions were shaken in a rotator for 24 hours at 15 rpm. The mixture was filtered with a syringe with a pore diameter of 0.45 µm and absorbance values were measured at 590 nm via UV-Vis Spectrophotometer. To explore the thermodynamic parameters of the adsorption process, the suspensions were shaken at 308-318 K in a water bath. In reusability experiments, after each adsorption cycle, the adsorbents were collected and washed, then regenerated by shaking with 5 mL of ethanol for 30 min. The adsorption capacity and adsorption ratio were calculated as in Equations 1 and 2.

$$q_e = \frac{(C_o - C_e) \times V}{m} \quad (1)$$

$$\text{Adsorption } (\%) = \frac{(C_o - C_e)}{C_o} x100 \quad (2)$$

Where q_e, C_o, Ce, V and m represent the adsorption capacity of CV at equilibrium (mg g^{-1}), initial CV concentration, CV concentration in equilibrium (mg L^{-1}), the volume of CV solution (L) and the UiO-66 mass (g), respectively.

3 Results and discussion

3.1 Characterization

FT-IR analysis was carried out to determine the functional groups in UiO-66 and the spectrum was provided

in Figure 1. Horti et al. reported that they obtained a sharp peak around 500 cm^{-1} corresponding to the stretching vibration of Zr-O [25]. The peak in this region in the spectrum can be attributed to inorganic structures arising from zirconium. The broad absorption band originating from both symmetric stretching of terephthalic acid and O-C-O asymmetry was noticed at 1400 cm^{-1} and 1537 cm^{-1}, respectively [26]. The peak at 1690 cm^{-1} is attributed to the N-H stretching absorption due to dimethylformamide which could not be rinsed from the adsorbent surface [27]. The peaks obtained in the range of 3500-4000 cm^{-1} indicate the presence of -OH and -NH_2 vibrations [28,29].

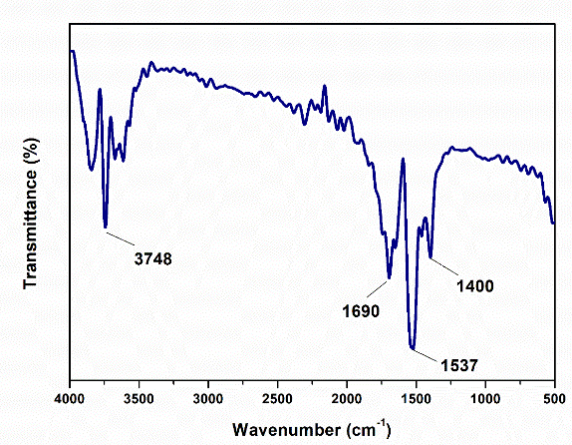

Figure 2. FT-IR spectrum of UiO-66 nanoparticle

To evaluate the crystallinity and phase purity of UiO-66, X-ray diffraction (XRD) analysis was performed as shown in Figure3. UiO-66 exhibits dominant peaks at 2θ=15.98°, 17.53°, 26.25°, 28.12°, 39.77° [30]. Based on the XRD pattern, the peaks obtained confirm the cubic crystal structure of UiO-66 [31]. The resulting diffractogram shows a pure and perfectly crystallized UiO-66 structure [32]. The intensity and sharpness of the peaks indicate that the synthesis was successful and that characteristic crystalline phases are located. Finally, it is clearly seen that no amorphous structure or other phase was formed during the synthesis step.

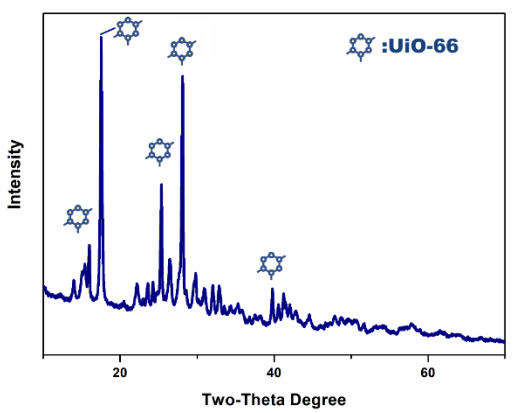

Figure 3. XRD pattern of UiO-66 sorbent

SEM analysis was performed to characterize the surface morphology and grain structure of the UiO-66 nanoparticles. Figure4 reveals that the UiO-66 particles were composed of cube-shaped nanocrystals resembling uniform spherical structures. It was clearly observed that no agglomeration occurs, the particles are independent of each other. It was found that the tiny particles were obtained in the range of 96.81 nm-103.24 nm. These results support that UiO-66 MOF was successfully synthesized by solvothermal technique. Chen et al. reported that UiO-66 consisted of cube-shaped crystals in the solvothermal synthesis carried out at 120 °C for 24 h. Moreover, it is seen from the SEM images that they obtained particles above 100 nm [33]. In this respect, it is concluded that temperature and reaction time significantly affect the particle structure of the obtained product in solvothermal synthesis. Han et al. reported that the particle size and structural morphology of UiO-66 can be controlled by utilizing hydrogen fluoride (HF). The particles obtained were between 150 nm and 7 µm in the HF-added system. They also reported that by adjusting the concentration of $ZrCl_4$ and H_2BDC, the structural morphology of MOF turned from a truncated cube to a cuboctahedron [31]. According to the results in the literature, it can be deduced that MOF structures are controllable, tunable and can be obtained in the desired crystal structure.

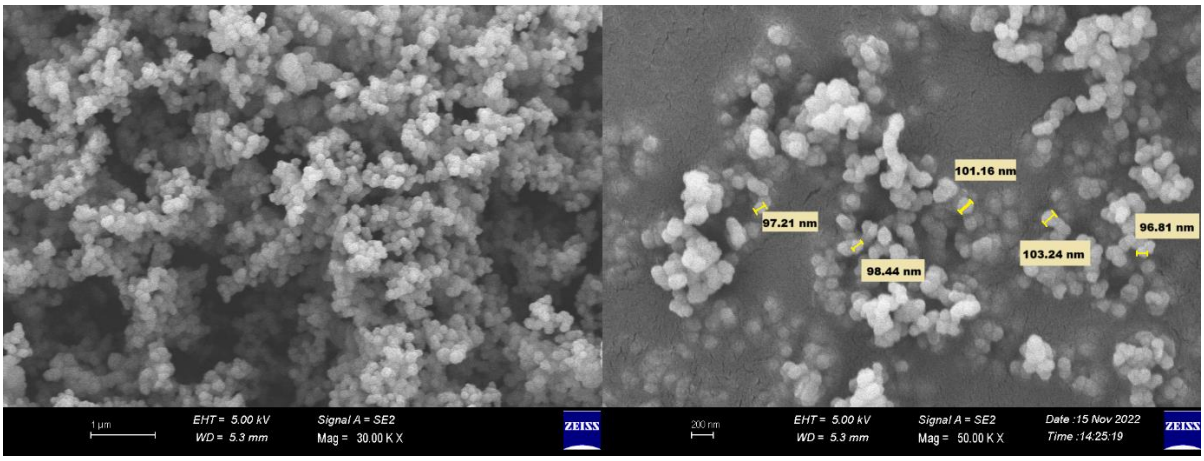

Figure 4. SEM images of UiO-66 (Magnification rates: x30000(left) and x50000(right))

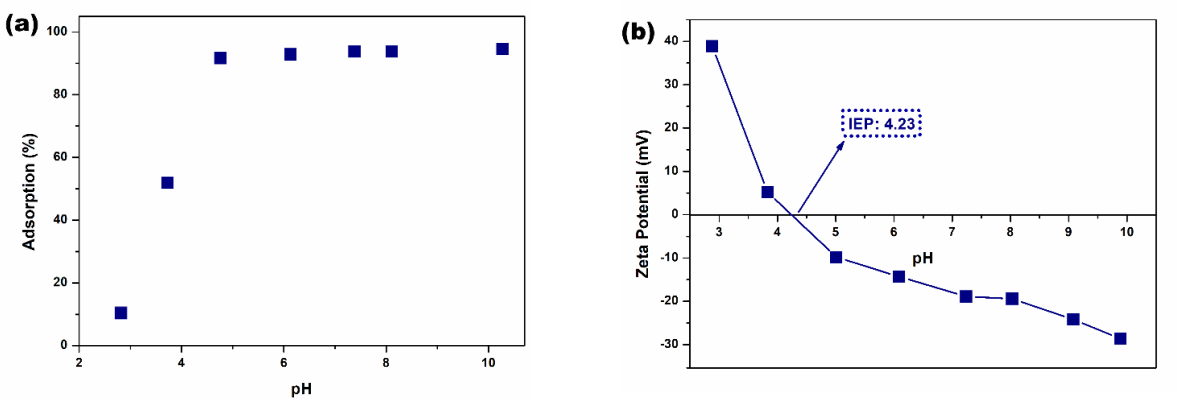

(a) (b)

Figure 5. (a) Solution pH effects on CV adsorption and (b) isoelectric point of UiO-66

The large surface area of adsorbent materials is favorable for the interaction of adsorbate molecules with enough active sites. According to the BET analysis, the specific surface area of the synthesized UiO-66 was found as 1107 m^2 g^{-1}. UiO-66 specific surface areas measured in various reports in the literature can be listed as follows; 1204 m^2 g^{-1} [1], 666.5 m^2 g^{-1} [34], 485.9 m^2 g^{-1} [35], 274.2 m^2 g^{-1} [36], 1198 m^2 g^{-1} [29], 854 m^2 g^{-1} [37]. As the prepared UiO-66 particles are nanoscale and have a large surface area, it supports them to be used in adsorption processes and to exhibit superior adsorption performance.

3.2 pH effect

The removal efficiency of the adsorbent is highly dependent on the ambient pH when the surface charge changes. The CV adsorption performance of UiO-66 nanoparticles was investigated at pH values in the range 2.82-10.27. The results were presented in Figure 5 (a). To adjust the pH of the CV solutions, 0.1 M NaOH or HCl solution was added. When the CV pH ranged from 2.82 to 4.76, a sharp increase in the adsorption rate of UiO-66 was obtained. The excess of H^+ ions in the solution decreased CV adsorption at low pHs. The zeta potential measurement results of the UiO-66 sorbent are presented in Figure 5 (b) and the isoelectric point (IEP) was found as 4.23. The sorbent surface was positively charged at pHs below the IEP and negatively charged at pHs above the IEP. In the experimental results, CV removal was extremely low at pH values below 4.23. At pH 2.82, 10.41% and at pH 3.73, 51.96% were achieved. However, when the pH was increased to 4.76, the CV removal reached 91.68%, therefore, it can be assumed that a significant electrostatic repulsion occurs as both the adsorbent surface and the components in the solution phase are positively charged. At pH 7.38, there were no H^+ ions in the solution phase and the removal percentage of cationic CV dye was 93.85%. The increase in the adsorption ratio from 91.68% to 93.85% at neutral pH proves the competitive adsorption of H^+ and cationic CV dye on the adsorbent surface in the acidic region. After pH 7.38, CV removal maintained a nearly constant. H^+ ion concentrations dropped as pH rose, but OH^- ion concentrations rose. All of the carboxylic groups on the adsorbent underwent a deprotonation process, which resulted in the binding sites of UiO-66 becoming negatively charged [38]. This is most likely what caused the increased adsorption capacity in basic pH dye solutions. As a result, the cationic CV molecules and the polyanionic adsorbent had robust and efficient electrostatic interactions. Furthermore, a high CV adsorption percentage results from the mutual repulsion of OH^- ions and anionic functions [39].

3.3 Adsorption kinetics

Experiments were conducted at various times to establish the minimum necessary adsorption time and to accomplish an economical and effective adsorption process. The interactions between the adsorbent and the adsorbate molecules in the solution were also examined, and the model equations were applied to the data that had been gathered. Experimental data were evaluated using pseudo-first-order (PFO), pseudo-second-order (PSO), Elovich and intra-particle diffusion (IPD) model equations (available in Equation (S4-7) in the supporting information file).

Figure 6 shows the fitting curves of the kinetic models to the experimental results. In the experiments performed between 5-90 min, it was observed that equilibrium was reached after 30 min and CV adsorption capacity did not increase between 30-90 min. At the end of 30 min, q_t value was 28.38 mg g^{-1}, while at the end of 90 min q_t values were calculated to be around 28.63 mg g^{-1}. In Figure 4, the curve that follows the experimental points most closely belongs to the PSO model.

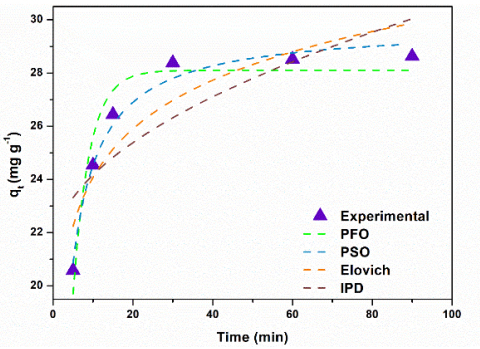

Figure 6. The fitting curves of kinetic models

Table 1 lists the kinetic model parameters, correlation (R^2) and chi-square (χ^2) coefficients. When R^2 and χ^2 values were compared, it was concluded that the PSO model was the best fitting model. The PSO model suggests that chemical interactions are dominant during adsorption processes. The q_e value calculated from the PFO model was found to be 28.10 mg g^{-1}, which is below the experimentally available adsorption capacity, while the q_e value calculated from the PSO model was found to be 29.78 mg g^{-1}. The α value was found to be 10^4 times greater than the β value, which proves the high affinity of the CV molecules to the UiO-66 surface and the rapidity of the adsorption process.

Table 1. Kinetic model coefficients of UiO-66.

Models	Coefficients	Value
PFO	k_1 (L min^{-1})	0.24
	qe (mg g^{-1})	28.10
	R^2	0.92
	χ^2	0.81
PSO	k_2 (g (mg min) $^{-1}$)	0.01
	q_e (mg g^{-1})	29.78
	R^2	0.98
	χ^2	0.21
Elovich	α (g (mg min) $^{-1}$)	$2.41x10^3$
	β (mg g^{-1})	0.38
	R^2	0.79
	χ^2	2.07
IPD	ki (g $mg^{-1}min^{-1/2}$)	0.93
	C	21.24
	R^2	0.60
	χ^2	4.11

3.4 Adsorption isotherm

10 mL of a 15–300 mg L^{-1} CV solution and 5 mg of adsorbent were used in isotherm experiments. The amount of CV adsorbed on UiO-66 as a function of CV equilibrium concentration is displayed in Figure 7. The experimental equilibrium results were subjected to the Langmuir, Freundlich, Temkin, and Dubinin-Radushkevich models, which are shown in Equation (S1-3). Although the Freundlich approach proposes that adsorption takes place in multilayer and non-equivalent energy adsorption sites, the Langmuir model hypothesizes that a monolayer adsorption consists on the sorbent in adsorption sites of equal energy. According to the Temkin model, when adsorbate molecules bind to the surface, the adsorption heat falls off linearly. The Dubinin-Radushkevich model is employed to show that adsorption on a heterogeneous sorbent surface takes place via a Gaussian energy dispersion mechanism.

The isotherm model parameters and compatibility coefficients are listed in Table 2. The calculated maximum monolayer adsorption capacity of CV on UiO-66 is calculated as 998.18 mg g^{-1}. The "1/n" Freundlich parameter ranges from 0 to 1, indicating that CV adsorption is favorable. The Dubinin Radushkevich isotherm model accurately describes UiO-66 based on correlation (R^2) and chi square (χ^2) coefficients. The calculated energy (E) was pointed out that the separation process has dominant physical interactions. The analyzed results also demonstrated that UiO-66 is an effective adsorbent for organic dye adsorption.

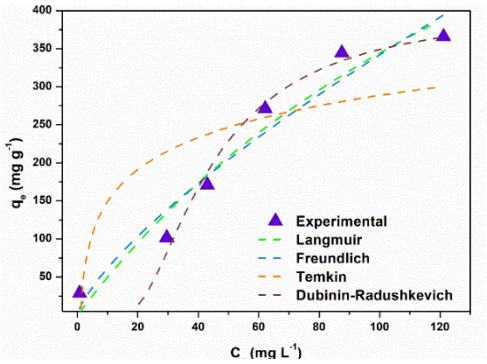

Figure 7. CV adsorption isotherm model fitting curves

Table 2. CV adsorption isotherm parameters.

Models	Coefficients	Value
Langmuir Isotherm	q_{max} (mg g^{-1})	998.18
	K_L (L m g^{-1})	$5.3x10^{-3}$
	R^2	0.95
	χ^2	978.76
Freundlich Isotherm	K_F (L g^{-1})	11.20
	n	0.74
	R^2	0.93
	χ^2	$1.2x10^3$
Temkin Isotherm	K_T (L mol^{-1})	1.18
	b_T (J mol^{-1})	40.93
	R^2	0.63
	χ^2	$6.8x10^3$
Dubinin-Radushkevich Isotherm	q_{max} (mg g^{-1})	403.32
	E (J mol^{-1})	26.37
	β (mol^2 J^2)	$1.4x10^3$
	R^2	0.98
	χ^2	418.67

3.5 Adsorption thermodynamic

The system temperature affects the adsorption processes obviously. Accordingly, the temperature effect on CV adsorption was investigated in the range of 308- 328 K. The thermodynamic parameters were calculated by using Eqs. (S9-12) and listed in Table 3. A decrease in K_d values was observed with increasing temperature and this was due to the increase in the amount of CV remaining in the solution when the temperature of the adsorption system increased. Negative ΔG^o values are indicated to spontaneous nature of CV removal. Additionally, the negative ΔH^o value means that CV adsorption is an exothermic character, furthermore ΔS^o gives insight into the irregularity of adsorbate-adsorbent interactions. Sadoq et al. reported that they obtained a spontaneous and exothermic process in CV adsorption with raw chitin [40].

Table 3. Thermodynamic parameters of UiO-66.

T(K)	K_d	ΔG^o (kJ mol^{-1})	ΔH^o (kJ mol^{-1})	ΔS^o (J $(mol\ K)^{-1}$)
308	20.23	-7.70		
318	10.18	-6.13	-46.30	-128.92
328	6.57	-5.13		

3.6 *Reusability*

The length of the useful life of adsorbent materials is of great importance from an economic perspective. In this framework, adsorption/desorption studies were carried out to analyze how many batches of UiO-66 could be used. 5 mg adsorbent was shaken with 10 mL of 15 mg L^{-1} CV solution for 30 min, collected at the end of the time, washed with distilled water and regenerated by shaking with 5 mL ethanol for 30 min and then applied to adsorption with CV again. The results are shown in Figure 8 with spent UiO-66 sorbent. While CV removal was 94.83% in the first cycle, it decreased to 80.04% at the end of the fifth cycle. After the first adsorption process, the recovered CV amount was 81.23%, whereas only 33.27% of CV could be desorbed after the last batch. It is clearly seen that relatively high removal rate can be achieved even at the end of the fifth cycle. Nevertheless, the present rate of decrease can be attributed to the fact that some CV molecules are not perfectly desorbed from the surface and various bonds are affected by chemical interactions (pseudo-second order compatibility) and break down. It can provide higher desorption efficiencies by using solvent mixtures instead of a single solvent.

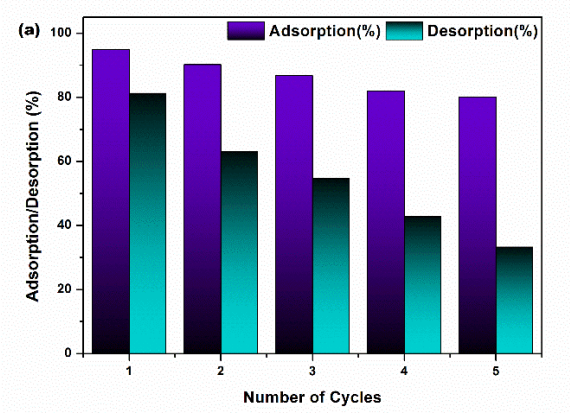

(a)

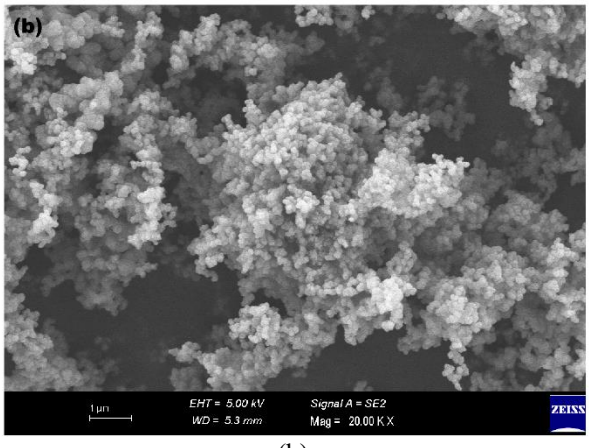

(b)

Figure 8. (a) Reusability of UiO-66 and (b) spent UiO-66 sorbent.

In addition, operating desorption for longer periods of time or applying different temperatures can improve desorption performance. On the other hand, SEM analysis was performed to examine whether there were morphological changes on the surface of the adsorbent particles after five cycles (Figure 8(b)). The fact that the surface does not change clearly before and after the adsorption/desorption cycles shows that UiO-66 is robust against dye molecules and organic solvent.

3.7 *Comparison with other studies*

Adsorbents from different classes were compared with their maximum CV adsorption capacities and surface areas and the results are presented in Table 4. CV adsorption capacities were obtained as 77.66 mg g^{-1} for chitosan and ionic liquid doped sulfonated PEEK (Ch-IL@SPEEK), 84.7 mg g^{-1} for titania nanoparticle doped carbon spheres (TNTs@Cs) and 469.55 mg g^{-1} for activated carbon obtained from Moroccan Moringa oleifera biomass (MMO-AC). When an evaluation is made for nanoparticle and/or metal-organic lattice adsorbents, it is clearly seen that MOF systems multiply the adsorption potential. It was reported that there were 109.23 mg g^{-1} for green tea nanoparticles (GTNP), 6750.58 mg g^{-1} for Ti-MOF-doped biomass (CMC/MIL-125@CS) and 827.54 mg g^{-1} for ZIF-8-doped lignosulfonate/diethylenetriaminepentaacetic acid (SLS/DTPA@ZIF-8). In this study, 998.18 mg g^{-1} CV adsorption capacity of UiO-66 nanoparticles with 1107 m^2 g^{-1} surface area is excellent compared to other adsorbents with longer and stepwise production processes in the literature. Although it is not an inexpensive material, UiO-66, which has a shorter operating process (30 min) and higher adsorption capacity, carries a preferable profile in terms of its superior performance and the possibility of reuse.

Table 4. CV adsorption capacity comparison

Adsorbent	S_{BET} (m^2 g^{-1})	q_{max} (mg g^{-1})	References
Ch-IL@SPEEK	-	77.66	[15]
TNTs@Cs	79.042	84.7	[41]
MMO-AC	1394.89	469.55	[42]
GTNP	15.925	109.23	[43]
CMC/MIL-125@CS	4.962	6750.58	[17]
SLS/DTPA@ZIF-8	-	827.54	[45]
UiO-66	1107	998.18	This study

4 Conclusion

In summary, solvothermally synthesized UiO-66 nanoparticles were employed as an adsorbent for CV removal. FT-IR, XRD, SEM, BET, and zeta potential measurements were conducted, whereas the structure of the prepared MOF was investigated. The equilibrium time of CV adsorption was determined to be 30 min, and the adsorption processes were confirmed to be consistent with the PSO kinetic model. In the isotherm analysis, the CV adsorption model was found to be compatible with the Dubinin-Raduskevich isotherm, and the maximum monolayer adsorption capacity calculated using the Langmuir model was 998.18 mg g^{-1}. CV adsorption was found to be low at acidic pH, and surface charge proved to be the major adsorption mechanism. By examining the influence of temperature, it was discovered that the CV adsorption

process was exothermic and spontaneous. The findings showed that zirconium-based MOFs are nanoparticles with a high adsorption capacity and the ability to rapidly achieve the equilibrium of CV dye. Future research could focus on increasing the reusability of UiO-66 nanoparticles by exploring different regeneration techniques to improve desorption efficiency. Furthermore, performance studies on real wastewater samples will further demonstrate its practical applicability in environmental remediation.

Acknowledgment

The author is grateful to Sally Kareem Abdulrazzaq and Hülya Sena Erdinç for their kind supports.

Conflict of interest

The author reported no possible conflicts of interest.

Similarity rate (iThenticate): 17%

References

[1] Y. Zhang, Q. Ruan, Y. Peng, G. Han, H. Huang, C. Zhong, Synthesis of hierarchical-pore metal-organic framework on liter scale for large organic pollutants capture in wastewater, J. Colloid Interface Sci. 525, 39–47, 2018. https://doi.org/10.1016/j.jcis.2018.04.063.

[2] G. Crini, Non-conventional low-cost adsorbents for dye removal : A review, Bioresour. Technol. 97, 1061–1085, 2006. https://doi.org/10.1016/j.biortech.2005.05.001.

[3] D. Iqbal, R. Ullah, M. Ilyas, R. Zhao, X. Ning, Fabrication and adsorption characteristics of cuprammonium cellulose-based membranes for removing anionic and cationic dyes, Colloids Surfaces A Physicochem. Eng. Asp. 705, 135692, 2005. https://doi.org/10.1016/j.colsurfa.2024.135692.

[4] A. Naifar, M. Bouzid, Physics statistical analysis of crystal violet adsorption onto activated bamboo fiber powder : Insights from thermodynamic functions, Mater. Chem. Phys. 329, 130110, 2025. https://doi.org/10.1016/j.matchemphys.2024.130110.

[5] G. Tang, H. Mo, L. Gao, Y. Chen, X. Zhou, Adsorption of crystal violet from wastewater using alkaline-modified pomelo peel-derived biochar, J. Water Process Eng. 68, 106334, 2024. https://doi.org/10.1016/j.jwpe.2024.106334.

[6] N. Kanmaz, M. Buğdaycı, Promoting photo-fenton catalytic performance of novel NiZrO3-type perovskite: Optimization with response surface methodology, J. Mol. Struct. 1295, 2024. https://doi.org/10.1016/j.molstruc.2023.136718.

[7] M. Wasim, A. Sabir, M. Shafiq, R.U. Khan, Mussel inspired surface functionalization of polyamide membranes for the removal and adsorption of crystal violet dye, Dye. Pigment. 206, 110606, 2022. https://doi.org/10.1016/j.dyepig.2022.110606.

[8] N. Kanmaz, M. Buğdaycı, P. Demircivi, Exploring photocatalytic tetracycline removal performance under simulated sunlight irradiation : Milling time effect on metallic reduction of MnO / ZrO 2 mixed oxide, Ceram. Int. 50, 44598–44608, 2024. https://doi.org/10.1016/j.ceramint.2024.08.308.

[9] Ö. Tuna, E. Bilgin Simsek, Promoted peroxymonosulfate activation into ferrite sites over perovskite for sunset yellow degradation: Optimization parameters by response surface methodology, Opt. Mater. 142, 2023. https://doi.org/10.1016/j.optmat.2023.114122.

[10] M. Zahmatkesh, S. Nourbakhsh, A. Toolabi, Z. Bonyadi, Biodegradation of crystal violet dye by Saccharomyces cerevisiae in aqueous medium, Heliyon. 9, e19460, 2023. https://doi.org/10.1016/j.heliyon.2023.e19460.

[11] F. Atmani, M. Mehdi, I. Akkari, N. Yeddou-mezenner, Adsorption ability of sugar scum as industrial waste for crystal violet elimination : Experimental and advanced statistical physics modeling, Surfaces and Interfaces. 54, 105166, 2024. https://doi.org/10.1016/j.surfin.2024.105166.

[12] N. Kanmaz, P. Demircivi, Superstable cellulose-supported clay-based methylene blue hybrid pigment encapsulated with porous TiO2 : Processing by adsorption strategy, Dye. Pigment. 220, 111764, 2023. https://doi.org/10.1016/j.dyepig.2023.111764.

[13] Ş. Karadirek, H. Okkay, Statistical modeling of activated carbon production from spent mushroom compost, J. Ind. Eng. Chem. 63, 340–347, 2018. https://doi.org/10.1016/j.jiec.2018.02.034.

[14] N. Kanmaz, M. Buğdaycı, P. Demirçivi, Investigation on structural and adsorptive features of BaO modified zeolite powders prepared by ball milling technique: Removal of tetracycline and various organic contaminants, Microporous Mesoporous Mater. 354, 2023.https://doi.org/10.1016/j.micromeso.2023.112566.

[15] M. Yılmazoğlu, N. Kanmaz, P. Demircivi, Constructing the synergistic effects of chitosan and ionic liquid on SPEEK polymer for efficient adsorption of crystal violet dye, Int. J. Biol. Macromol. 271, 2024. https://doi.org/10.1016/j.ijbiomac.2024.132638.

[16] B. Yardımcı, N. Kanmaz, M. Buğdaycı, P. Demircivi, Synthesis of CuBDC metal-organic framework supported zinc oxide via ball-milling technique for enhanced adsorption of Orange-II, Surfaces and Interfaces. 46, 2024. https://doi.org/10.1016/j.surfin.2024.104122.

[17] N. Kanmaz, B. Yardimci, P. Demircivi, In situ synthesis of MIL-125 on cinnamon stick and improved via carboxymethyl cellulose : A sustainable approach for super-high crystal violet adsorption, J. Colloid Interface Sci. 678, 366–377, 2025. https://doi.org/10.1016/j.jcis.2024.09.035.

[18] J. Canivet, A. Fateeva, Y. Guo, B. Coasne, D. Farrusseng, Water adsorption in MOFs : fundamentals and applications, Chem. Soc. Rev. 43, 5594–5617, 2014. https://doi.org/10.1039/c4cs00078a.

[19] N. Kanmaz, P. Demircivi, Adsorption of tetracycline using one-pot synthesis zirconium metal-organic framework (UiO-66) decorated hydroxyapatite, J. Mol. Liq. 397, 124171, 2024. https://doi.org/10.1016/j.molliq.2024.124171.

[20] C. Zhang, L. Ma, X. Xi, Z. Nie, Separation of molybdenum and tungsten using selective adsorption with zirconium based metal organic framework, J. Taiwan Inst. Chem. Eng. 165, 105802, 2024. https://doi.org/10.1016/j.jtice.2024.105802.

[21] C. Zhang, L. Ma, X. Xi, Z. Nie, Adsorption and separation performance of tungsten and molybdenum on modified zirconium based metal organic frameworks UiO-66-CTAB, J. Environ. Chem. Eng. 12, 113401, 2024. https://doi.org/10.1016/j.jece.2024.113401.

[22] A. Assafi, Y. Aoulad, E. Hadj, R.S. Almufarij, L. Hejji, N. Raza, P. Luis, B. Souhail, Ultrasound-assisted adsorption of organic dyes in real water samples using zirconium(IV) -based metal-organic frameworks UiO-66-NH2 as an adsorbent, Heliyon. 9, 1–18, 2023. https://doi.org/10.1016/j.heliyon.2023.e22001.

[23] H. Zhao, X. Huang, D. Jiang, P. Ren, R. Wang, Z. Liu, G. Li, S. Pu, Post-synthetic modification of zirconium-based metal-organic frameworks for enhanced simultaneous adsorption of heavy metal ions and organic dyes, J. Solid State Chem. 339 (2024) 124987. https://doi.org/10.1016/j.jssc.2024.124987.

[24] D. Lan, H. Zhu, J. Zhang, F. Wang, Y. Zheng, One step synthesis of a novel Co-doped UiO-66 adsorbent for superior adsorption of organic dyes from wastewater, Process Saf. Environ. Prot. 188, 1058–1068, 2024. https://doi.org/10.1016/j.psep.2024.05.122.

[25] N.C. Horti, M.D. Kamatagi, S.K. Nataraj, M.N. Wari, S.R. Inamdar, Structural and optical properties of zirconium oxide (ZrO2) nanoparticles : effect of calcination temperature, Nano Express. 1, 010022, 2020. https://doi.org/10.1088/2632-959X/ab8684.

[26] H. Dadashi, R. Halladj, A. Karimi, K. Sharifi, Enhancing oxidative desulfurization catalytic performance of metal – organic frameworks UiO-66 (Zr) by post-synthetic with the creation of active sites, Inorg. Chem. Commun. 170, 113340, 2024. https://doi.org/10.1016/j.inoche.2024.113340.

[27] X. Fang, S. Wu, Y. Wu, W. Yang, Y. Li, J. He, P. Hong, High-efficiency adsorption of norfloxacin using octahedral UiO-66-NH2 nanomaterials : Dynamics , thermodynamics , and mechanisms, Appl. Surf. Sci. 518, 146226, 2021. https://doi.org/10.1016/j.apsusc.2020.146226.

[28] R. Heu, M.A. Ibrahim, U. States, E. Protection, C. Yoshimura, Photocatalytic nanofiltration membrane using Zr-MOF/GO nanocomposite photocatalytic nanofiltration membrane using Zr-MOF/GO nanocomposite with high-flux and anti-fouling properties, Catalysts. 10, 2020. https://doi.org/10.3390/catal10060711.

[29] Y.L. Wang, S. Zhang, Y.F. Zhao, J. Bedia, J.J. Rodriguez, C. Belver, UiO-66-based metal organic frameworks for the photodegradation of acetaminophen under simulated solar irradiation, J. Environ. Chem. Eng. 9, 106087, 2023. https://doi.org/10.1016/j.jece.2021.106087.

[30] A. Naeem, T. Saeed, M. Sayed, B. Ahmad, T. Mahmood, M. Farooq, F. Perveen, Chitosan decorated zirconium metal-organic framework for collaborative adsorption and photocatalytic degradation of methylene blue and methyl orange, Process Saf. Environ. Prot. 176, 115–130, 2023. https://doi.org/10.1016/j.psep.2023.06.012.

[31] Y. Han, M. Liu, K. Li, Y. Zuo, Y. Wei, S. Xu, G. Zhang, C. Song, Z. Zhang, X. Guo, Facile synthesis of morphology and size-controlled zirconium metal–organic framework UiO-66: the role of hydrofluoric acid in crystallization, CrystEngComm. 17, 6434–6440, 2015. https://doi.org/10.1039/C5CE00729A.

[32] A. Farid, H. Nageh, T.S. Soliman, A. Khalid, N.M. M., M. Taha, Explore the physical properties of the synthesized UiO-66, Zn-BiOBr, and Zn-BiOBr/UiO-66 heterostructures for optical applications, J. Alloys Compd. 1010, 177467, 2025. https://doi.org/10.1016/j.jallcom.2024.177467.

[33] C. Chen, D. Chen, S. Xie, H. Quan, X. Luo, L. Guo, Adsorption behaviors of organic micropollutants on zirconium metal-organic framework UiO-66 : Analysis of surface interactions, ACS Appl. Mater. Interfaces. 9, 41043–41054, 2017. https://doi.org/10.1021/acsami.7b13443.

[34] A. Zhang, B. Liu, M. Liu, Z. Xie, D. Wang, G. Feng, The adsorption properties of defect controlled metal-organic frameworks of UiO-66, Sep. Purif. Technol. 270, 118842, 2011. https://doi.org/10.1016/j.seppur.2021.118842.

[35] X. He, F. Deng, T. Shen, L. Yang, D. Chen, J. Luo, X. Luo, X. Min, F. Wang, Exceptional adsorption of arsenic by zirconium metal-organic frameworks : Engineering exploration and mechanism insight, J. Colloid Interface Sci. 539, 223–234, 2019. https://doi.org/10.1016/j.jcis.2018.12.065.

[36] S. Zhuang, C. Rong, J. Wang, Adsorption of diclofenac from aqueous solution using UiO-66-type metal-organic frameworks, Chem. Eng. J., 2018. https://doi.org/10.1016/j.cej.2018.11.150.

[37] J. Yu, X. Wang, Y. Wang, X. Xie, H. Xie, N. Vorayos, J. Sun, Heating-induced adsorption promoting the efficient removal of toluene by the metal-organic framework UiO-66 (Zr) under visible light, J. Colloid Interface Sci. 653, 1478–1487, 2024. https://doi.org/10.1016/j.jcis.2023.09.164.

[38] Q. Tan, X. Jia, R. Dai, H. Chang, M. Wai, H. Chen, Synthesis of a novel magnetically recyclable starch-based adsorbent for efficient adsorption of crystal violet dye, Sep. Purif. Technol. 320, 124157, 2023. https://doi.org/10.1016/j.seppur.2023.124157.

[39] A. Rahmatpour, B. Shoghinia, A.H. Alizadeh, A self-assembling hydrogel nanocomposite based on xanthan gum modified with SiO2 NPs and HPAM for improved adsorption of crystal violet cationic dye from aqueous solution, Carbohydr. Polym. 330, 121819, 2024. https://doi.org/10.1016/j.carbpol.2024.121819.

[40] M. Sadoq, H. Atlas, S. Imame, A. Kali, A. Amar, I. Loulidi, M. Jabri, B. Sadoq, M. Ouchabi, P. Sannasi, F. Boukhlifi, Elimination of crystal violet from aqueous

solution by adsorption on naturel polysaccharide : Kinetic, isotherm, thermodynamic studies and mechanism analysis, Arab. J. Chem. 17, 105453, 2024. https://doi.org/10.1016/j.arabjc.2023.105453.

[41] A.M.E. Mohammed, A. Kotb, M.M.S. Sanad, M. Abdel-Hakim, A.S.A. Ahmed, Enhanced adsorption of carbon sphere by doping with titania nanotubes for crystal violet removal: isotherm, kinetics, and thermodynamic studies, RSC Adv. 14, 31332–31347, 2024. https://doi.org/10.1039/d4ra04889j.

[42] Y. Raji, A. Nadi, I. Mechnou, M. Saadouni, O. Cherkaoui, S. Zyade, High adsorption capacities of crystal violet dye by low-cost activated carbon prepared from Moroccan Moringa oleifera wastes: Characterization, adsorption and mechanism study, Diam. Relat. Mater. 135, 109834, 2023. https://doi.org/10.1016/j.diamond.2023.109834.

[43] B. Yardımcı, N. Kanmaz, Ecosafe-design of carboxymethyl cellulose encapsulated polyphenolic bio-nanocomposite valorized for sustainable industrial textile dye removal, J. Environ. Chem. Eng., 115321, 2025. https://doi.org/10.1016/j.jece.2025.115321.

[44] L. Yang, L. Bao, Y. Zhong, C. Hao, J. Chen, J. Wu, X. Wang, Fa[brication of in situ metal-organic framework grown on sodium lignosulphonate hydrogel for removal of Pb2+, methylene blue and crystal violet from aqueous solution, J. Clean. Prod. 434, 139831, 2024. https://doi.org/10.1016/j.jclepro.2023.139831.